Journal of Alloys and Compounds 509 (2011) 9340–9345

Contents lists available at ScienceDirect

Journal of Alloys and Compounds

journal homepage: www.elsevier.com/locate/jallcom

Magnetic entropy changes at early stages of nanocrystallization in amorphous $Fe_{90}Zr_7B_3$ ribbons

J. Świerczek[a,*], T. Mydlarz[b]

[a] Institute of Physics, Częstochowa University of Technology, al. Armii Krajowej 19, 42-200 Częstochowa, Poland
[b] International Laboratory of High Magnetic Fields and Low Temperatures, ul.Gajowicka 95, 53-421 Wrocław, Poland

ARTICLE INFO

Article history:
Received 30 May 2011
Accepted 11 July 2011
Available online 23 July 2011

Keywords:
Amorphous and nanostructured materials
Mössbauer spectroscopy
Magnetization
Magnetic entropy changes

ABSTRACT

Microstructure, revealed by transmission electron microscopy and conventional Mössbauer spectroscopy, magnetization versus magnetizing field induction and temperature and isothermal magnetic entropy changes in the as-quenched and subjected to annealing at T_{a1} = 723 K for 2 or 3 h and at T_{a2} = 743 K for 2.5 h of $Fe_{90}Zr_7B_3$ amorphous alloy are studied. In the as-quenched state the medium range ordered regions are observed. The annealing at T_{a1} leads to early stages of crystallization and nanograins with different diameter embedded in amorphous matrix are formed. At the Curie point of the amorphous phase they are magnetically decoupled and behave like superparamagnetic particles. The Curie point of the residual amorphous phase shifts towards higher temperature as compared to the as-quenched state due to the Invar like effect. The peak of the isothermal magnetic entropy changes appears at the Curie temperature of the main amorphous phase. Their values at the maximum applied field of 0.75 T equals to 0.32 J/kg K^{-1} in the as-quenched alloy and remain almost unchanged after early stages of nanocrystallization. After the annealing at T_{a2} the peak of the entropy changes distinctly decreases. Such behavior is ascribed to the biphasic character of the sample. The main amorphous phase and ordered one, which in some circumstances can be treated as an assembly of superparamagnetic particles, contribute to the total magnetic entropy changes.

1. Introduction

Magnetic entropy changes during the isothermal magnetization process and the magnetocaloric effect understood as the temperature change during adiabatic magnetization or demagnetization have been extensively investigated in magnetic materials due to their potential application as refrigerants [1]. The maximum of the magnetic entropy changes occur at the temperature of the ferromagnetic–paramagnetic phase transition [2], so searching for magnetic materials with the Curie point near room temperature is essential for application of these materials in refrigerant appliances. The large magnetic entropy changes near the ambient temperature have been found in several compounds: $Gd_5Ge_2Si_2$ [3], MnAs [4] and MnFe(P,As) [5]. These changes arise from the first order magnetic–crystallographic phase transition which is, however, accompanied by significant thermal and magnetic hysteresis producing irreversible magnetic entropy changes. Contrary to this, in soft magnetic materials these irreversible entropy changes can be avoided owing to the low coercivity. Among soft magnetic materials the transition metals based amorphous and nanocrystalline alloys have gained the greatest attention due to their excellent magnetic properties and high electrical resistivity [6–12]. Although the magnetic entropy change in these, exhibiting the second order phase transition, materials is not as large as in materials with the first order phase transition, the magnetic entropy change peak is broader which enables the higher refrigerant capacity.

NANOPERM-type Fe–M–B–(Cu) (M = Zr, Hf and Nb) amorphous alloys are known as precursors of extremely soft nanocrystalline magnetic materials obtained by conventional heat treatments [13]. The nanocrystalline material consists of nanometric crystalline α-Fe grains embedded in the residual amorphous matrix. The magnetic properties of this material depend on both the volume fraction of the crystalline phase and temperature. When the amount of the crystalline phase is small (less than 20%) and the matrix is in the paramagnetic state the superparamagnetic relaxations take place [14,15]. Averaging out of the crystalline anisotropy in the material containing 60–70% of the crystalline phase leads to the excellent soft magnetic properties. The magnetic entropy changes in nanocrystalline materials, usually measured near the Curie temperature of the amorphous matrix [10,11], are smaller than in amorphous precursors and depend on the volume fraction of the crystalline phase. The peaks of magnetic entropy changes show distinct broadening comparatively to these peaks for the amorphous material.

* Corresponding author. Tel.: +48 34 325 0795; fax: +48 34 325 0795.
E-mail address: swiercz@wip.pcz.pl (J. Świerczek).

0925-8388/$ – see front matter © 2011 Elsevier B.V. All rights reserved.
doi:10.1016/j.jallcom.2011.07.033

Recently, the magnetic entropy changes in two series of the amorphous $Fe_{90-x}Zr_{10}B_x$ ($3 \le x \le 9$), $Fe_{93-x}Zr_7B_x$ ($0 \le x \le 13$) alloys [16] and independently in $Fe_{90}Zr_7B_3$ alloy [17] in the as-quenched state have been reported.

The goal of this paper is to study the microstructure, the temperature and field dependence of the magnetization and magnetic entropy changes at early stages of nanocrystallization in the amorphous $Fe_{90}Zr_7B_3$ alloys subjected to the conventional annealing in vacuum.

2. Experimental

The amorphous $Fe_{90}Zr_7B_3$ alloy in the form of ribbons, 20 μm thick and 15 mm wide, was prepared by a rapid quenching on a single roller. The square 15 mm × 15 mm, and disc 3 mm in diameter specimens were subjected to annealing at temperature T_{a1} = 723 K for 2 h or 3 h and at T_{a2} = 743 K for 2.5 h in vacuum of 1.33×10^{-3} Pa. The microstructure of the as-quenched and annealed samples was investigated by the transmission electron microscopy and the Mössbauer spectroscopy. A JEM 3010 microscope working in the high-resolution regime was used. The transmission Mössbauer spectra were collected at both liquid nitrogen (77 K) and room temperatures (300 K) by means of a conventional constant acceleration spectrometer with a ^{57}Co(Rh) radioactive source of 100 mCi in activity. The spectrometer was calibrated and the isomer shift (IS) was determined with respect to the polycrystalline α-Fe foil. Spectra fittings were carried out using the NORMOS package written by Brand [18]. Due to the closeness of the Curie temperature of the residual amorphous matrix after annealing at T_{a1} = 723 K to the ambient temperature and spectra sensitivity to temperature changes special care was taken to maintain the temperature at the same level (300 ± 1) K during spectra recording. The magnetization versus temperature at the magnetizing field of 0.75 T was measured by a force Sucksmith's type magnetometer for samples consisting of 5 discs 3 mm in diameter arranged along the ribbon edge. The isothermal magnetization curves as a function of the magnetizing field induction in the range 0–0.75 T were recorded for the same samples by a vibrating sample magnetometer (VSM) in the temperature range 77–300 K and by mentioned above Sucksmith's type magnetometer in the range 300–450 K. All magnetization measurements were done for samples in the as-quenched state and after annealing.

3. Results and discussion

The transmission electron microscopy image of the as-quenched $Fe_{90}Zr_7B_3$ ribbon is shown in Fig. 1a. The corresponding electron diffraction pattern is shown as an inset in the left top corner of this figure. The microstructure and selected area diffraction pattern are characteristic of amorphous state, although the high-resolution regime reveals the medium range ordered (MRO) regions denoted by white rings in Fig. 1a. MRO regions become the nuclei of the crystalline grains during primary crystallization. More detail analysis of MRO regions is reported in [17]. Fig. 1b displays the microstructure image and electron diffraction pattern for the samples annealed at T_{a1} = 723 K for 2 h. The crystalline grains with diameter in the range 6–34 nm embedded in the amorphous intergranular phase can be clearly seen. The average distance between adjacent grain boundaries is about 60 nm. The electron diffraction pattern, beside broad rings coming from amorphous phase, contains very bright reflexes which distances from the centre of pattern are related to the reciprocal of the interplane distances in α-Fe phase. Comparing the MRO regions to α-Fe grains (Fig. 1a and b) it can be seen that MRO regions exhibit continuous order–disorder space structural transition, whereas the abrupt grain boundaries are visible. No distinct changes in the microstructure and electron diffraction pattern for the sample subjected to the heat treatment at T_{a1} = 723 K for 3 h occur as compared to the structure of the specimen shown in Fig. 1b. The grain size range does not change but the average distance between adjacent grain boundaries decreases to 50 nm.

The transmission Mössbauer spectrum obtained at 300 K for the as-quenched $Fe_{90}Zr_7B_3$ alloy is presented in Fig. 2a. The spectrum typical of amorphous paramagnet is asymmetric indicating the correlation between IS and quadrupole splitting (QS). The QS distribution shown in Fig. 2b is derived assuming the linear dependence of IS on QS. Not vanishing value of probability for QS = 0 indicates the existence of a single line form component in the spectrum decomposition [17]. The spectra recorded for the samples subjected to the annealing at T_{a1} = 723 K for 2 h and 3 h are depicted in Fig. 2c and e, respectively. The best results of fitting are obtained when the spectra are decomposed into two components; a subspectrum with QS distribution related to the residual amorphous matrix (PP) and a single sextet corresponding to the crystalline phase (CP). The derived QS distributions for the samples annealed at T_{a1} = 723 K for 2 and 3 h are displayed in Fig. 2d and f, respectively. Some parameters of the fittings are listed in Table 1. One can see that the hyperfine magnetic induction of the crystalline phase corresponds to α-Fe ferromagnetic phase, which is consistent with the discussed above electron microscopy observations. Moreover, the sextets areas take only 7 and 10% of the total spectrum areas for specimens heat treated at T_{a1} = 723 K for 2 and 3 h, respectively (Table 1). These quantities are lowered in comparison with the area taken by the subspectrum related to the MRO regions in the as-quenched state, which equals to about 8% of the total spectrum area [17]. In Fig. 3 the transmission Mössbauer spectrum obtained at 77 K for the specimen annealed at T_{a1} = 723 K for 3 h and its decomposition into a single sextet and a subspectrum with magnetic hyperfine field distribution corresponding to the crystalline α-Fe and ferromagnetic amorphous phase, respectively, are shown. Moreover, the relative sextet area of the crystalline α-Fe phase is larger when the spectrum is recorded at 77 K. For example, the area

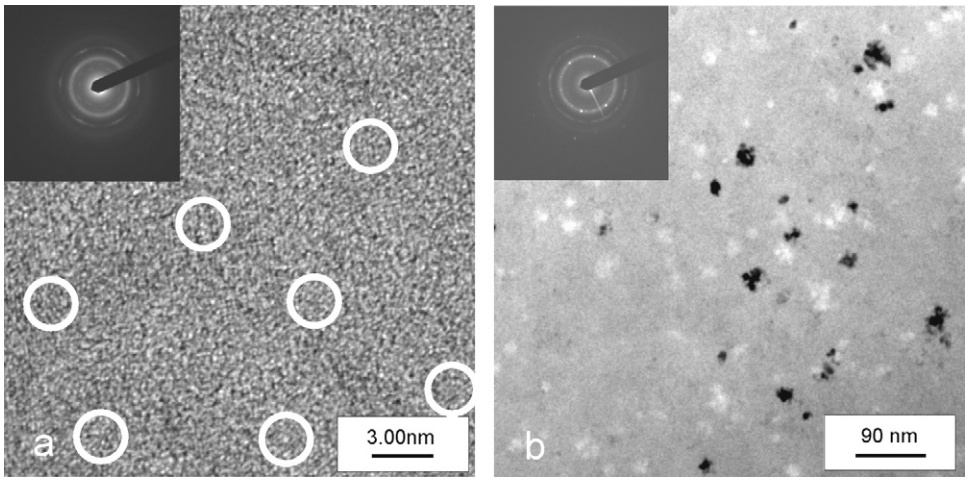

Fig. 1. Transmission electron microscopy images and selected area diffraction patterns for $Fe_{90}Zr_7B_3$ alloy in the as-quenched state (a) and after the annealing at T_{a1} = 723 K for 2 h (b).

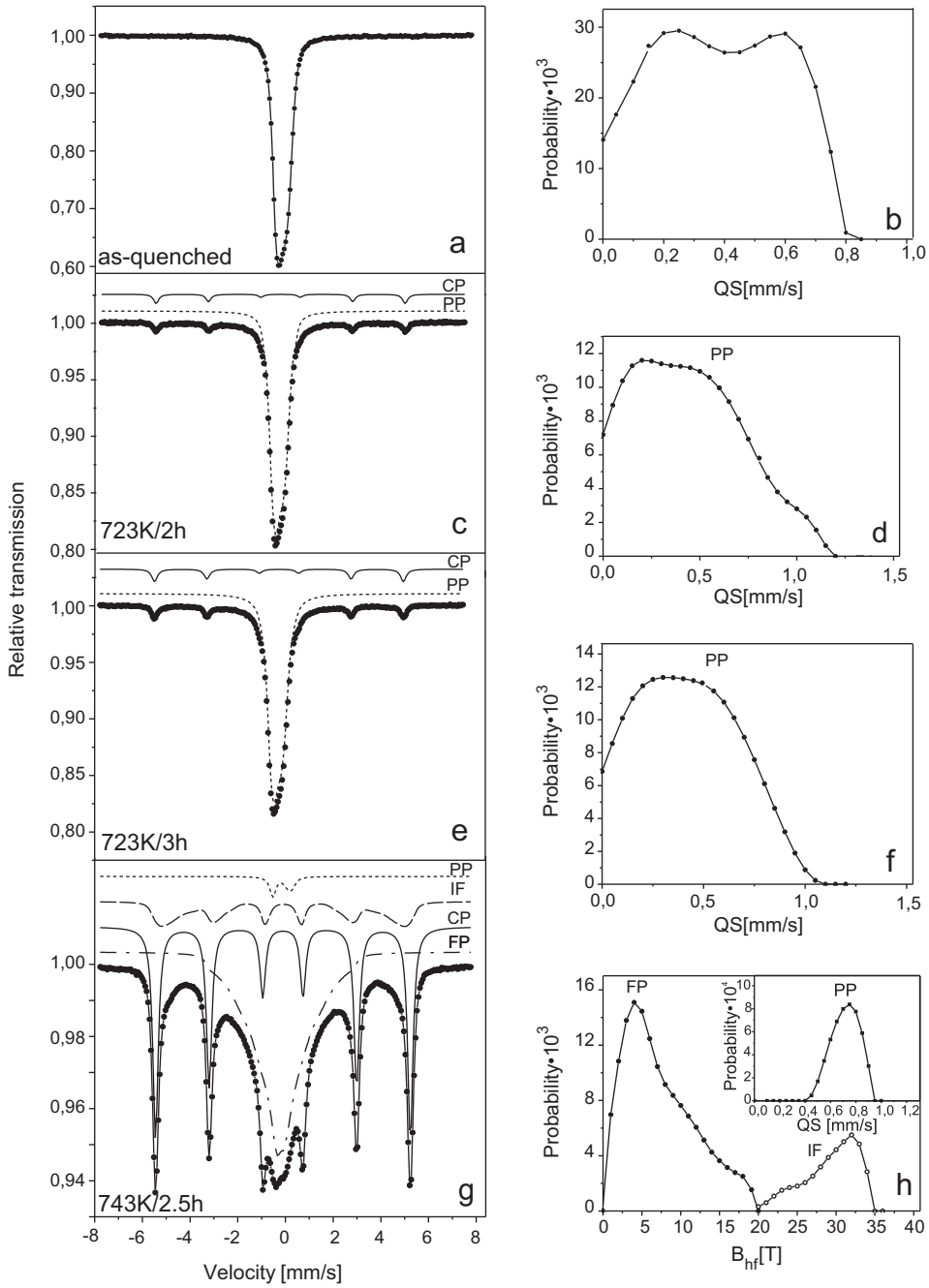

Fig. 2. Transmission Mössbauer spectra at 300 K, their decompositions and corresponding hyperfine parameters distributions for $Fe_{90}Zr_7B_3$ alloy in the as-quenched state (a and b), after the annealing at T_{a1} = 723 K for 2 h (c and d) and 3 h (e and f), and after the annealing at T_{a2} = 743 K for 2.5 h (g and h). CP denotes crystalline phase, PP – paramagnetic amorphous phase, FP – ferromagnetic amorphous phase, IF interface.

of the subspectrum corresponding to the crystalline phase after the annealing at T_{a1} = 723 K for 3 h is about 15% of the total spectrum area (Fig. 3 and Table 1). It is worth noticing that the hyperfine field induction, B_{cr}, and IS_{cr} for the crystalline phase are typical of α-Fe phase at the liquid nitrogen temperature. Because of the fact that in the "thin-absorber" approximation the relative area of the subspectrum is proportional to the relative number of ^{57}Fe atoms in the particular phase, the similar results for the relative area of the same phase should have been expected for the spectra recorded at 77 and 300 K. In order to elucidate this discrepancy the superparamagnetic behavior can be considered. After the heat treatment at T_{a1} = 723 K for 2 and 3 h the crystalline grains of α-Fe phase with diameters in the range 6–34 nm, embedded in the paramagnetic amorphous phase can be treated as an assembly of non interacting or weakly interacting particles if small dipolar interaction is taken into account. The critical diameter of a single magnetic domain α-Fe spherical particle is about 50 nm [19], so differing in size non interacting α-Fe grains are single domain particles. The relaxation time of the magnetization in a particle with BCC structure is given by the relation [20]:

$$\tau = \tau_0 \ \exp\left(\frac{KV}{4k_BT}\right) \quad (1)$$

where τ_0 is of the order of 10^{-10} s, K – the positive anisotropy constant, V – the volume of the particles, k_B – Boltzmann constant and T – the temperature. Taking into account the time scale of Möss-

Table 1
Some hyperfine parameters of the spectra decompositions shown in Figs. 2 and 3; $\overline{QS}$ – the average value of the quadrupole splitting in the paramagnetic phase, ΔQS – standard deviation of QS, $\bar{B}_{hf}$ – the average value of the hyperfine magnetic induction, ΔB_{hf} – the standard deviation of B_{hf}, B_{cr} – the hyperfine induction of the crystalline phase, $\overline{IS}$ – the mean value of the isomer shift related to the polycrystalline bulk α-Fe at room temperature, IS_{cr} – the isomer shift of the crystalline phase, A – relative area of the subspectrum in the total spectrum area. Uncertainties for the last significant figure are given in brackets.

Thermal history of the sample	Subspectrum	$\overline{QS}$ (mm/s)	ΔQS (mm/s)	$\bar{B}_{hf}$ (T)	ΔB_{hf} (T)	B_{cr} (T)	$\overline{IS}$ (mm/s)	IS_{cr} (mm/s)	A (%)
As-quenched	Doublets distribution	0.38(1)	0.20(1)				−0.080(1)		100
723 K/2 h	Doublets distribution	0.47(1)	0.32(1)				−0.077(1)		93(1)
	Sextet					33.05(2)		−0.004(3)	7(1)
723 K/3 h	Doublets distribution	0.45(1)	0.29(1)				−0.080(1)		90(1)
	Sextet					33.03(1)		−0.002(2)	10(1)
723 K/3h[a]	Sextets distribution			21.25(1)	7.07(1)		0.037(5)		85(1)
	Sextet					34.10(1)		0.098(2)	15(1)
743 K/2.5 h	Doublets distribution	0.70(1)	0.14(1)				−0.07(6)		2(1)
	Sextets distribution			7.35(1)	4.68(1)		−0.093(3)		49(1)
	Sextets distribution			29.25(1)	3.46(1)		0.02(1)		14(1)
	Sextet					33.14(1)		0.0006(3)	35(1)

[a] Measurements carried out at 77 K.

bauer spectroscopy $\tau_M = 5 \times 10^{-9}$ s [15], the anisotropy constant for α-Fe $K = 5 \times 10^4$ J/m^3 [19] and assuming the spherical shape of the particle one can calculate the critical diameter of 14 nm. It means that the particles with higher diameter (τ longer than τ_M) contribute to the subspectrum in the form of a sextet and the particles with lower diameter (τ shorter than τ_M) participate only in a single line formation. In other words, no every grain of α-Fe formed during heat treatment contributes to the single sextet subspectrum shown in Fig. 2c and e. In this way the estimation of the crystalline phase volume fraction from the relative areas of the subspectra may be misleading. At the temperature of 77 K the exchange coupling of the grains via ferromagnetic amorphous matrix takes place and collective magnetism occurs. One can believe that each grain participates in the single sextet formation depicted in Fig. 3a. The Mössbauer spectrum recorded at 300 K for the samples subjected to annealing at $T_{a2} = 743$ K for 2.5 h and corresponding hyperfine parameters distributions are displayed in Fig. 2g and h. The complicated spectrum is decomposed into four subspectra according to the procedure described in details in [21]: single sextet related to the crystalline α-Fe phase (CP), the subspectrum with sextet distribution connected to the interface (IP), the subspectrum with sextet distribution corresponding to ferromagnetic phase in amorphous matrix (FP) and the subspectrum with QS doublets distribution related to the paramagnetic phase in the residual amorphous matrix (PP). Some parameters of such decomposition are also listed in Table 1. The area of the single sextet related to the α-Fe phase takes 35% of the total spectrum area. For the best fitting the block of hyperfine magnetic induction distribution in the interfacial zone is necessary to introduce. The mean value of $\bar{B}_{hf}$ at ^{57}Fe nuclei occurring in the interface between crystalline grains and amorphous matrix is about 29.25 T and is somewhat lower than in α-Fe grains ($B_{cr} = 33.14$ T). The crystalline grains of the α-Fe phase seem to be magnetically coupled via almost ferromagnetic intergranular phase exhibiting the average magnetic hyperfine induction of $\bar{B}_{hf} = 7.35$ T at room temperature (Table 1).

In Fig. 4 the magnetization, at the constant magnetizing field induction of 0.75 T as a function of temperature in the range 77–670 K for $Fe_{90}Zr_7B_3$ alloy samples in the as-quenched state, after annealing at $T_{a1} = 723$ K for 2 and 3 h and after annealing at $T_{a2} = 743$ K for 2.5 h $Fe_{90}Zr_7B_3$ samples is presented. In all cases the magnetization decreases monotonically with temperature exhibiting the curves proper for biphasic systems. The Curie temperatures of the amorphous phases can be derived from the temperature dependence of magnetization at temperatures lower but close to the Curie point:

$$M(T) = M_o(0)\left(1 - \frac{T}{T_C}\right)^{\beta} \quad (2)$$

where M is the magnetization, $M_o(0)$ – the critical amplitude, T – temperature, T_C – Curie point and $\beta = 0.36$ is the critical

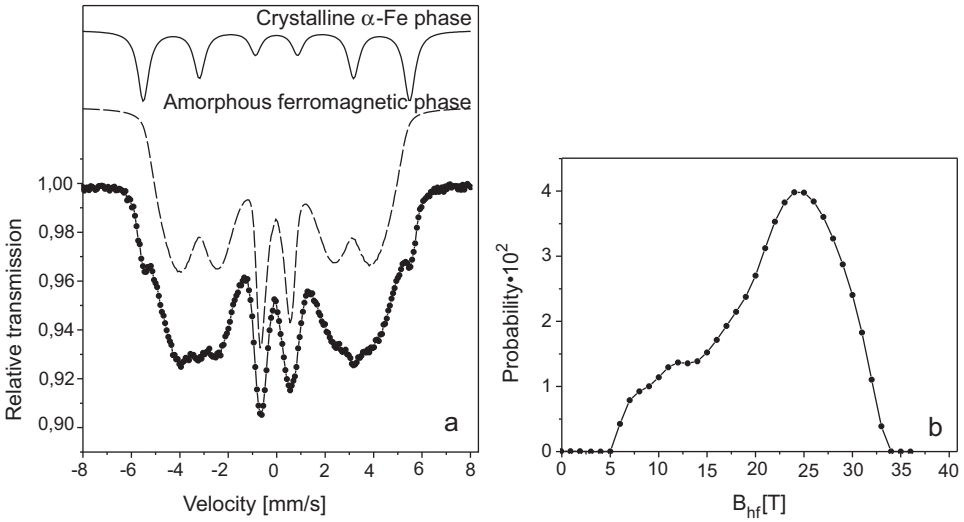

Fig. 3. Transmission Mössbauer spectrum taken at 77 K, its decomposition (a) and corresponding hyperfine field induction distribution of the amorphous phase (b) for $Fe_{90}Zr_7B_3$ alloy annealed at $T_{a1} = 723$ K for 3 h.

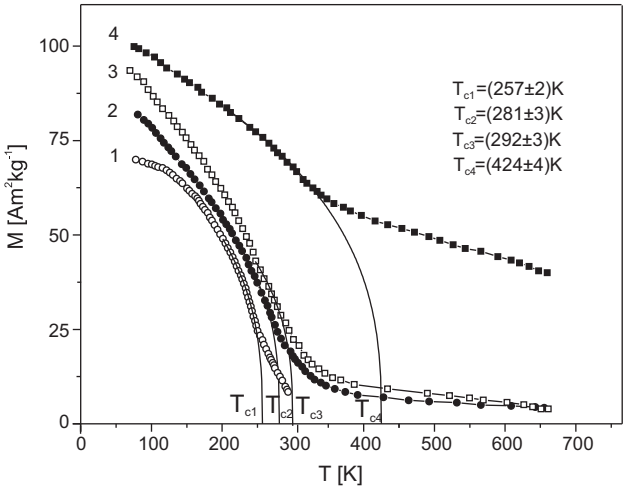

Fig. 4. Temperature dependence of unit mass magnetization at $B = 0.75$ T for $Fe_{90}Zr_7B_3$ alloy in the as-quenched state (curve1), after the heat treatment at $T_{a1} = 723$ K for 2 h (curve 2), 3 h (curve 3) and after the heat treatment at $T_{a2} = 743$ K for 2.5 h (curve 4). The black solid lines are magnetization versus temperature according to Eq. (2) dependences for Curie temperatures determination.

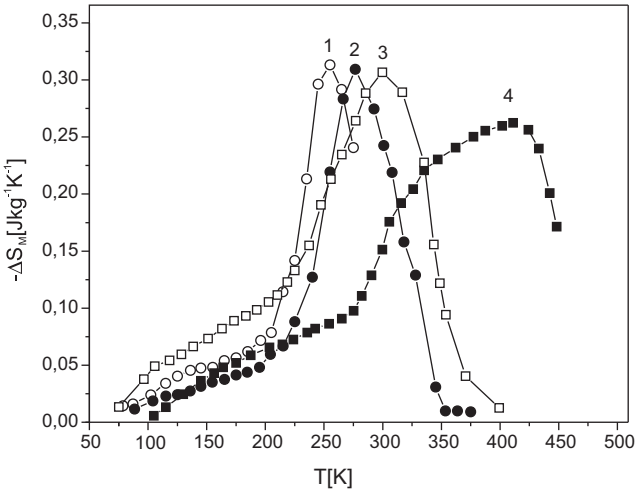

Fig. 6. Temperature dependence of the isothermal magnetic entropy changes at the maximum of magnetizing field induction of 0.75 T for $Fe_{90}Zr_7B_3$ alloy in the as-quenched state (curve 1), after the annealing at $T_{a1} = 723$ K for 2 h (curve 2), 3 h (curve 3) and after the heat treatment at $T_{a2} = 743$ K for 2.5 h (curve 4).

exponent for a Heisenberg ferromagnet. The relations given by the Eq. (2) are represented by solid black lines in Fig. 4. The derived Curie temperatures of the amorphous phases are equal to: $T_{C1} = (257 \pm 2)$ K in the as-quenched state, $T_{C2} = (281 \pm 3)$ K after the annealing at $T_{a1} = 723$ K for 2 h, $T_{C3} = (292 \pm 3)$ K after the annealing at $T_{a1} = 723$ K for 3 h and $T_{C4} = (424 \pm 4)$ K after the annealing at $T_{a2} = 743$ K for 2.5 h. The formation of α-Fe crystalline phase during heat treatment results in amorphous matrix poorer in iron than the parent amorphous alloy. The average distance between Fe atoms increases strengthening the exchange interaction as Fe–Fe distances are around the critical one of about 0.254 nm, somewhat larger than the Goldschmidt Fe diameter (0.248 nm) [22]. This invar like effect seems to be the origin of the Curie temperature changes in the amorphous residual matrix. It is worth pointing out that T_C changes are influenced not only by composition changes but by the exchange field penetration from BCC-Fe nanocrystallites into residual amorphous matrix, as well [23–25]. At early stages of nanocrystallization after the annealing at $T_{a1} = 723$ K the Curie point of the amorphous phase shifts towards room temperature but remains far below the Curie temperature of the crystalline phase (T_C of α-Fe phase equals to 1041 K). Fig. 5 displays for instance isothermal magnetization curves versus magnetizing field induction $\mu_0 H$ (μ_0 is the vacuum magnetic permeability and H – the magnetizing field strength) for a few temperatures from the range 80–360 K and for the sample of $Fe_{90}Zr_7B_3$ alloy heat treated at $T_{a1} = 723$ K for 3 h. Similar behaviors are observed for the sample in the as-quenched state and after the annealing at $T_{a1} = 723$ K for 2 h and at $T_{a2} = 743$ K for 2.5 h. From the isothermal magnetization curves the magnetic entropy changes, ΔS_M, can be calculated according to the Maxwell thermodynamic relation [2]:

$$\Delta S_M = \mu_0 \int_0^{H_{max}} \left(\frac{\partial M(T,H)}{\partial T} \right)_H dH = \int_0^{B_{max}} \left(\frac{\partial M(T,B)}{\partial T} \right)_B dB \quad (3)$$

where B is the magnetizing field induction. ΔS_M is computed using the numerical approximation of this equation described in details in [17]. The isothermal magnetic entropy changes versus the temperature for $Fe_{90}Zr_7B_3$ alloy in the as-quenched state, and after heat treatments are shown in Fig. 6. The maximum magnetizing field induction is $B_{max} = 0.75$ T in all cases. The maxima of $-\Delta S_M(T)$ occur at the Curie temperature of the amorphous phase. It can be seen that the maximum value of $-\Delta S_M$ is about 0.32 J/kg K^{-1} for the samples in the as-quenched state and remains almost unchanged after the annealing at $T_{a1} = 723$ K, i.e. $-\Delta S_M$ equals to 0.31 J/kg K^{-1} after the annealing for 2 h and 0.30 J/kg K^{-1} for 3 h, respectively. After the heat treatment at $T_{a2} = 743$ K the maximum of $-\Delta S_M$ remarkably decreases to the value of 0.26 J/kg K^{-1}. It is also visible that the width of the $-\Delta S_M(T)$ curves increases with the time and temperature of annealing. The specimens in the as-quenched state and after heat treatments at $T_{a1} = 723$ Kcan be considered as biphasic systems consisting of α-Fe MRO regions and the amorphous medium, and α-Fe crystalline phase in the residual amorphous matrix, respectively. The total field induced magnetic entropy changes for biphasic systems is the algebraic sum of the particular phases contributions [26]:

$$\Delta S_M = \Delta S_M^C + \Delta S_M^A \quad (4)$$

where ΔS_M^C and ΔS_M^A originate from the MRO regions or crystalline phase and from the amorphous phase, respectively. The magnetic entropy changes of the main amorphous phase decreases when additional ordered phase appears in the material. Moreover, if at the Curie point of the amorphous phase the magnetic decoupling between grains takes place and they behave like non interacting superparamagnetic particles, ΔS_M^C may be enhanced [27] especially

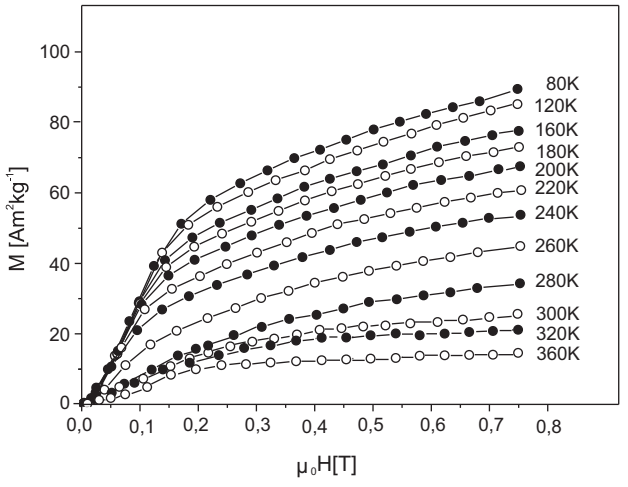

Fig. 5. Unit mass magnetization versus the magnetic induction of applied field for $Fe_{90}Zr_7B_3$ alloy annealed at $T_{a1} = 723$ K for 3 h.

at ΔS_M peak temperature leading only to the slight decrease of maxima entropy changes in the samples subjected to the annealing at T_{a1} = 723 K as compared to this behavior for the as-quenched state (curves 1–3 in Fig. 6). It is interesting to note that in these cases over the Curie point of the amorphous phases no irreversible magnetic entropy changes are produced because the magnetization without magnetic hysteresis occurs. The almost unchanged ΔS_M maxima shifted towards room temperature makes $Fe_{90}Zr_7B_3$ alloy be interesting as the magnetic refrigerant. The ribbons in the as-quenched state and after the annealing at T_{a1} = 723 K for 2 and 3 h working in a layered system can effectively "cover" a wide range of temperature near ambient one during magnetic refrigeration.

After annealing at T_{a2} = 743 K for 2.5 h the magnetic coupling between crystalline grains does not vanish even at the Curie temperature of the residual amorphous phase and domain structure is present. The magnetization process in crystalline grains and in the interfacial zone causes only negligible ΔS_M^C changes [10,11] indicating the decisive role of the amorphous phase in behavior of magnetic entropy changes and in this way ΔS_M shows lower maximum comparatively to the as-quenched state (curves 1 and 4 in Fig. 6).

4. Conclusions

From the investigations performed the following conclusion can be drawn:

- The high-resolution electron microscopy displays that MRO regions occur in the as-quenched $Fe_{90}Zr_7B_3$ alloy.
- After the annealing at T_{a1} = 723 K for 2 h the α-Fe crystalline grains with diameter in the range 6–34 nm embedded in the amorphous matrix are present. The average distance between the boundaries of the adjacent grains is about 60 nm.
- The transmission Mössbauer spectrum at 300 K in the as-quenched state of $Fe_{90}Zr_7B_3$ alloy, typical of amorphous paramagnets, can be presented as doublets distribution with not vanishing probability for QS equal to 0. After annealing at T_{a1} = 723 K for 2 and 3 h spectra at 300 K can be decomposed into single sextets corresponding to α-Fe crystalline phase and doublet distributions related to paramagnetic amorphous matrix. Due to the grain diameter distribution and superparamagnetic relaxation some grains contribute to the total spectrum in the form of a single line and other in the form of a single sextet.
- For the best fitting of the spectrum obtained at 300 K for the sample of $Fe_{90}Zr_7B_3$ alloy heat treated at T_{a2} = 743 K for 2.5 h a subspectrum related to the interfacial zone should be introduced.
- The Curie temperature of the amorphous phase $T_{C1} = (257 \pm 2)$ K in $Fe_{90}Zr_7B_3$ alloy shifts to $T_{C2} = (281 \pm 3)$ K and $T_{C3} = (292 \pm 3)$ K after the annealing at T_{a1} = 723 K for 2 and 3 h, respectively. The Curie point of the residual amorphous matrix, T_{C4}, in the sample subjected to the heat treatment at T_{a2} = 743 K for 2.5 h equals to 424 ± 4 K. The increase of T_C with time and annealing temperature is connected with invar like characteristics of the material. The tuning of the Curie point can be achieved not only by minor compositional change, but by proper annealing of the material, as well.
- The peak of entropy changes occurs at the Curie temperature of the amorphous medium in all samples. The width of $-\Delta S_M(T)$ curves depends on temperature and time of the sample annealing.
- The values of the maximum entropy changes after the annealing at T_{a1} = 723 K, which lead to early stages of nanocrystallization remain almost unchanged in comparison to the as-quenched $Fe_{90}Zr_7B_3$ alloy and can be ascribed to the existence of ordered phase consisting of non interacting single magnetic domain particles and exhibiting superparamagnetic relaxation at temperatures higher or equal to the Curie point of the main amorphous phase.

Acknowledgment

The authors would like to thank to Prof. J. Lelątko from Institute of Materials Science, University of Silesia, for transmission electron microscopy observations.

References

[1] E. Brück, J. Phys. D: Appl. Phys. 38 (2005) R381–R391, and reference therein.
[2] V.K. Pecharsky, K.A. Gschneidner Jr., J. Magn. Magn. Mater. 200 (1999) 44–56.
[3] A.O. Pecharsky, K.A. Gschneidner, V.K. Pecharsky, J. Appl. Phys. 93 (2003) 4722–4728.
[4] H. Wada, T. Asano, J. Magn. Magn. Mater. 290-291 (2005) 703–705.
[5] E. Brück, M. Ilyn, A.M. Tishin, O. Tegus, J. Magn. Magn. Mat. 290–291 (2005) 8–13.
[6] D. Wang, K. Peng, B. Gu, Z. Han, S. Tang, W. Qin, Y. Du, J. Alloy Compd. 358 (2003) 312–315.
[7] P. Didukh, A. Ślawska–Waniewska, J. Magn. Magn. Mater. 254-255 (2003) 407–409.
[8] V. Franco, J.S. Blázquez, M. Millián, J.M. Borrego, C.F. Conde, A. Conde, J. Appl. Phys. 101 (2007), 09C5031-3.
[9] V. Franco, C.F. Conde, A. Conde, L.F. Kiss, Appl. Phys. Lett. 90 (2007), 0525091-3.
[10] I. Škorvánek, J. Kováč, J. Marcin, P. Švec, D. Janičkovič, Mater. Sci. Eng. A 449–451 (2007) 460–463.
[11] C. Gómez-Polo, L.M. Socolovsky, J.C. Denardin, M. Knobel, J.I. Pérez-Landazábal, V. Recarte, J. Magn. Magn. Mater. 316 (2007) e876–e878.
[12] A. Kolano-Burian, M. Kowalczyk, R. Kolano, R. Szymczak, H. Szymczak, M. Polak, J. Alloy Compd. 479 (2009) 71–73.
[13] K. Suzuki, A. Makino, A. Inoue, T. Masumoto, J. Appl. Phys. 74 (1993) 3316–3322.
[14] T. Kemény, D. Kaptás, J. Balogh, L.F. Kiss, T. Pusztai, I. Vincze, J. Phys.: Condens. Matter 11 (1999) 2841–2847.
[15] J. Olszewski, Hyperfine Interact. 131 (2000) 83–90.
[16] Y. Wang, X. Bi, Appl. Phys. Lett. 95 (2009), 262501-3.
[17] J. Świerczek, J. Magn. Magn. Mater. 322 (2010) 2696–2702.
[18] R.A. Brand, Nucl. Instrum. Methods: Phys. Res. B28 (1987) 398–416.
[19] R.C. O'Handley, in: R.C. O'Handley (Ed.), Modern Magnetic Materials. Principles and Applications, John Wiley and Sons, New York, 2000, pp. 303–307.
[20] I. Eisenstein, A. Aharoni, Phys. Rev. B 16 (1977) 1278–1284.
[21] M. Miglerini, J-M. Greneche, J. Phys.: Condens. Matter 9 (1997) 2303–2319.
[22] J.M. Barandiarán, P. Gorria, I. Orúe, M.L. Fdez-Gubieda, F. Plazaola, A. Hernando, Phys. Rev. B 54 (1996) 3026–3029.
[23] J.S. Garitaonandria, D.S. Schmool, J.M. Barandiarán, Phys. Rev. B 58 (1998) 12147–12158.
[24] I. Škorvánek, J. Kováč, J-M. Grenèche, J. Phys. Condens. Matter 12 (2000) 9085–9093.
[25] K. Suzuki, J.M. Cadogan, J. Appl. Phys. 87 (2000) 7095–7099.
[26] J.J. Ipus, J.S. Blázquez, V. Franco, A. Conde, J. Alloy Compd. 496 (2010) 7–12.
[27] R.D. McMichael, R.D. Shull, L.J. Swartzendruber, L.H. Bennett, J. Magn. Magn. Mater. 111 (1992) 29–33.